## 1. INTRODUCTION

Flash x-rays have been produced by several different methods, and various generators have been developed corresponding to specific radiographic objectives.[1-3] Currently, the maximum photon energy has been increased to approximately 1 MeV using multiple-stage Marx pulse generators[1,2] in order to produce hard x-rays for military studies. In soft x-ray generators,[4-8] high-intensity single generators with large capacity condensers were originally developed. Subsequently, repetitive generators[9-12] have been developed, and the repetition rate has been increased to sub-kilohertz using a cold-cathode triode.

Recently, soft x-ray lasers have been produced by a gas-discharge capillary,[13-16] and the laser pulse energy substantially increased in proportion to the capillary length. These kinds of fast discharges can generate hot and dense plasma columns with aspect ratios approaching 1000:1. However, it is difficult to increase the laser photon energy to 10 keV or beyond. Because there are no x-ray resonators in the high photon energy region, new methods for increasing coherence will be desired in the future.

By forming weakly ionized linear plasma[17-21] using plate and rod targets, we confirmed irradiation of intense K-series characteristic x-rays from the plasma axial direction. In these experiments, because we employed a transmission-type x-ray spectrometer utilizing an x-ray film, it was difficult to determine the relative intensities of the characteristic x-rays. In former experiments, because we have succeeded in producing fairly intense and sharp K-series characteristic x-rays, monochromatic x-rays should be produced using a filter.

In this paper, we describe a plasma flash x-ray generator utilizing a rod-target radiation tube, used to perform a preliminary experiment for generating intense and sharp monochromatic x-rays by forming a linear copper plasma cloud around a fine target.

## 2. GENERATOR

### 2.1 High-voltage circuit

Figure 1 shows a block diagram of the high-intensity plasma flash x-ray generator. This generator consists of the following essential components: a high-voltage power supply, a high-voltage condenser with a capacity of approximately 200 nF, a turbo-molecular vacuum pump, a krytron pulse generator as a trigger device, and a flash x-ray tube. In this generator, a low-impedance transmission line is employed in order to increase maximum tube current. The high-voltage main condenser is charged to 50 kV by the power supply, and electric charges in the condenser are discharged to the tube after triggering the cathode electrode with the trigger device. The plasma flash x-rays are then produced.

### 2.2 X-ray tube

The x-ray tube is a demountable cold cathode triode that is connected to the turbo-molecular pump with a pressure of approximately 1 mPa (Fig. 2). This tube consists of the following major parts: a pipe-shaped carbon cathode with a bore diameter of 10.0 mm, a trigger electrode made from copper wire, a stainless steel vacuum chamber, a nylon insulator, a polyethylene terephthalate (Mylar) x-ray window 0.25 mm in thickness, and a rod-shaped copper target 3.0 mm in diameter with a tip angle of 60°. The distance between the target and cathode electrodes is approximately 20 mm, and the trigger electrode is set in the cathode electrode. As electron beams from the cathode electrode are roughly converged to the target by the electric field in the tube, evaporation leads to the formation of a weakly ionized linear plasma, consisting of copper ions and electrons, around the fine target.

### 2.3 Principle of characteristic x-ray irradiation

In the linear plasma, bremsstrahlung photons with energies higher than the K-absorption edge are effectively absorbed and are converted into fluorescent x-rays (Fig. 3). The plasma then transmits the fluorescent rays easily, and bremsstrahlung rays with energies lower than the K-edge are also absorbed by the plasma. In addition, because bremsstrahlung rays are not emitted in the direction opposite that of electron acceleration, intense characteristic x-rays are generated from the plasma-axial direction.

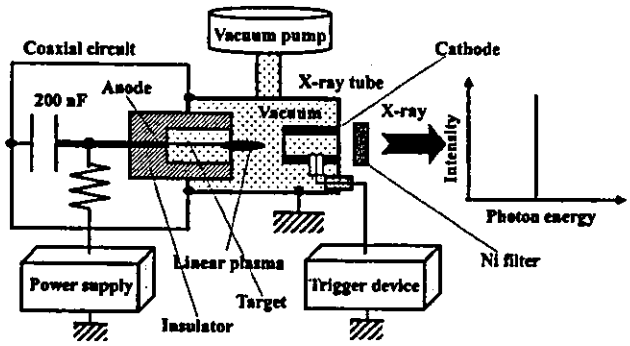


Figure 1: Block diagram of the high-intensity plasma flash x-ray generator.

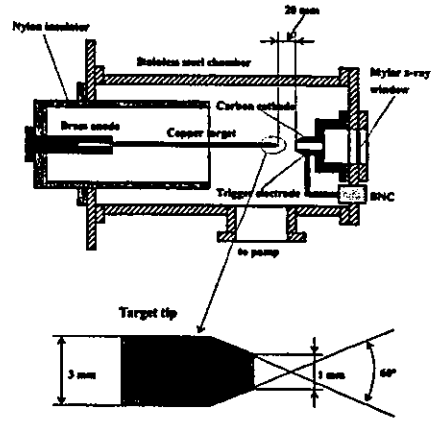


Figure 2: Schematic drawing of the flash x-ray tube with a rod target.

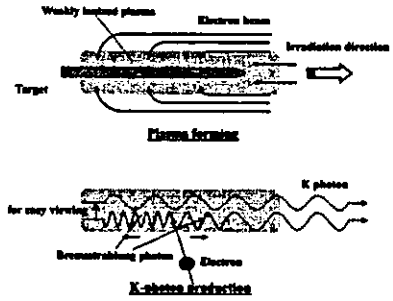


Figure 3: K-photon irradiation from the plasma.

## 3. CHARACTERISTICS

### 3.1 Tube voltage and current

Tube voltage and current were measured by a high-voltage divider with an input impedance of 1 GΩ and a current transformer, respectively. Figure 4 shows the time relation for the tube voltage and current. At the indicated charging voltages, they roughly displayed damped oscillations. When the charging voltage was increased, both the maximum tube voltage and current increased. At a charging voltage of 50 kV, the maximum tube voltage was almost equal to

the charging voltage of the main condenser, and the maximum tube current was approximately 15 kA.

### 3.2 X-ray output

X-ray output pulse was detected using a combination of a plastic scintillator and a photomultiplier using a 10 μm-thick monochromatic copper filter (Fig. 5). The x-ray pulse height substantially increased with corresponding increases in the charging voltage. The x-ray pulse widths were about 700 ns, and the time-integrated x-ray intensity per pulse measured by a thermoluminescence dosimeter (Kyokko TLD Reader 1500 utilizing MSO-S elements without energy compensation) had a value of about 30 μC/kg at 1.0 m from the x-ray source with a charging voltage of 50 kV.

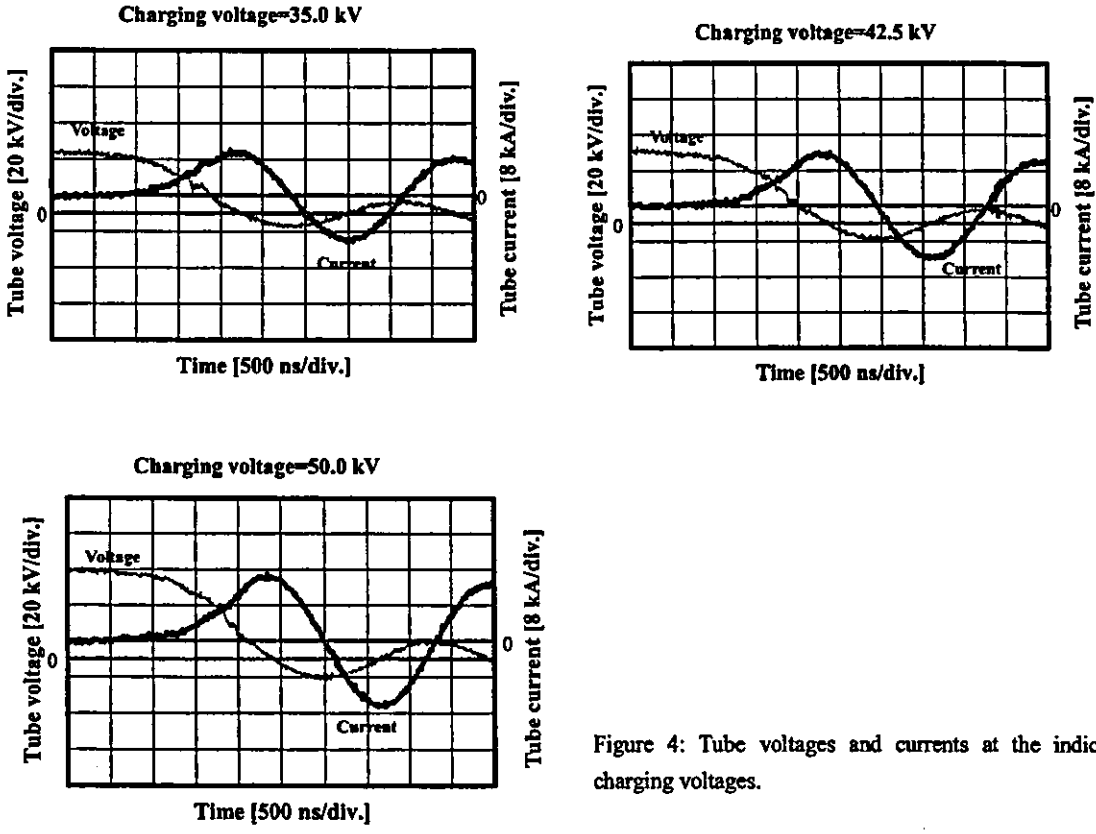


Figure 4: Tube voltages and currents at the indicated charging voltages.

### 3.3 X-ray source

In order to measure images of the plasma x-ray source, we employed a pinhole camera with a hole diameter of 100 μm (Fig. 6). When the charging voltage was increased, the plasma x-ray source grew, and both spot dimension and intensity increased.

### 3.4 X-ray spectra

X-ray spectra from the plasma source were measured by a transmission-type spectrometer (Fig. 7) with a lithium

fluoride curved crystal 0.5 mm in thickness. The spectra were taken by a computed radiography (CR) system[22] (Konica Regius 150) with a wide dynamic range, using the filter, and relative x-ray intensity was calculated from Dicom digital data. Figure 8 shows measured spectra from the copper target using the filter. In fact, we observed sharp lines of K-series characteristic x-rays such as lasers, while bremsstrahlung rays were hardly detected at all. The characteristic x-ray intensity of the $K_\alpha$ line substantially increased with corresponding increases in the charging voltage, and the $K_\beta$ line was absorbed by the filter.

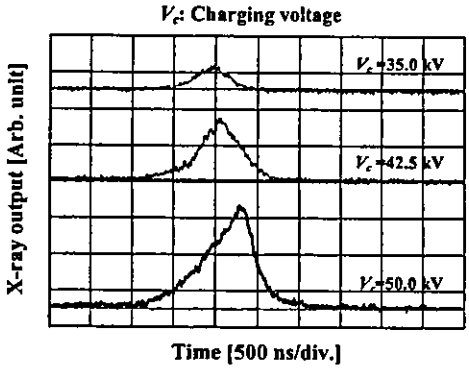


Figure 5: X-ray outputs measured by a plastic scintillator with changes in the charging voltage.

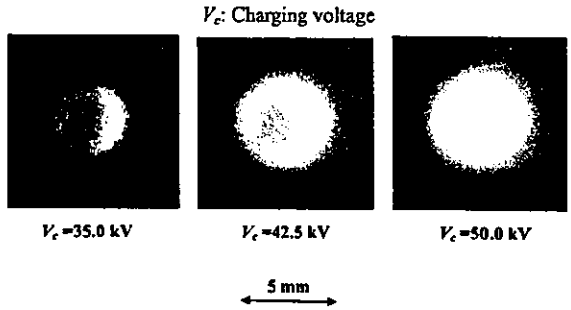


Figure 6: Images of the plasma x-ray source measured by a pinhole of 100 μm from the plasma axial direction.

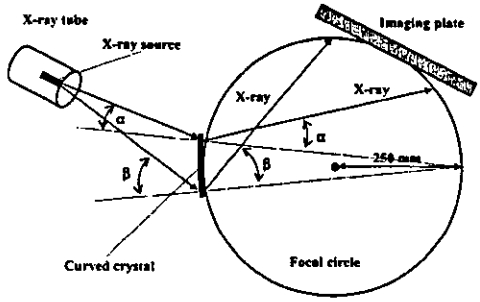


Figure 7: Transmission-type spectrometer with a lithium fluoride curved crystal and an imaging plate.

### 3.5 X-ray divergence by slits

In order to ascertain the difference in characteristics between x-rays from a conventional tube and these from the plasma tube, we employed two lead slits in order to measure the divergence of the x-rays (Fig. 9). As compared with incoherent x-rays from a conventional tube with a tungsten target, the characteristic x-rays from the linear plasma were diffused greatly after passing through the two slits (Fig. 10).

### 3.6 Rectilinear power

Figure 11 shows the experimental setup for measuring the rectilinear power of the $K_\alpha$ lines from a conventional tube and that from the plasma tube using the spectrometer previously described. In this experiment, we measured the coefficient $(I_k/I_t)$ of peak diffraction intensity of $K_\alpha$ $(I_k)$ to transmission intensity $(I_t)$. In the case where the

conventional tube was used, we employed the filter with a tube voltage of 17 kV. When the charging voltage was increased, the linear plasma grew, and the $I_k/I_t$ decreased to approximately 0.004. As compared with a value of 0.009 obtained by the conventional tube, the rectilinear power may be increased, because the values from the plasma were approximately halved.

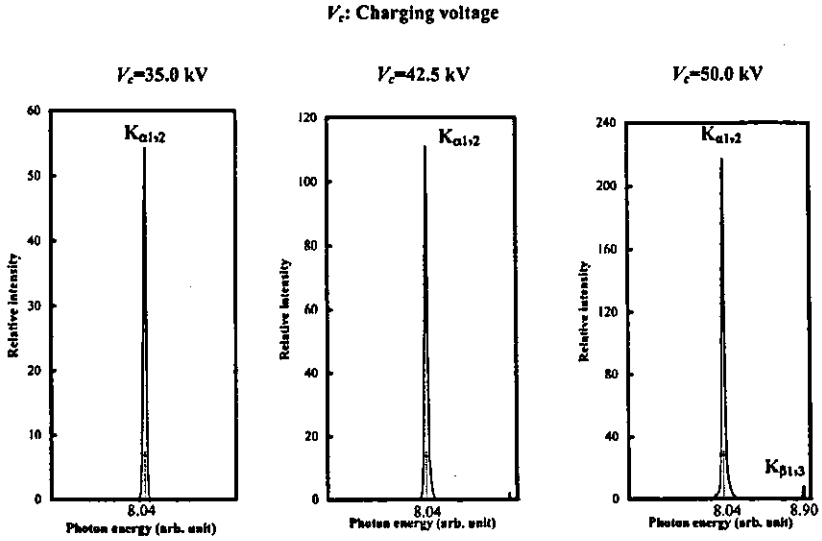


Figure 8: X-ray spectra from weakly ionized copper plasma according to changes in the charging voltage and to insertion of a nickel monochromatic filter.

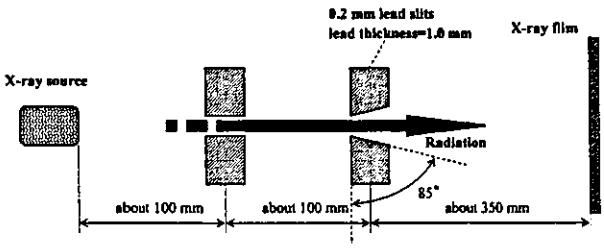


Figure 9: Experimental setup for measuring x-ray divergence using two lead slits.

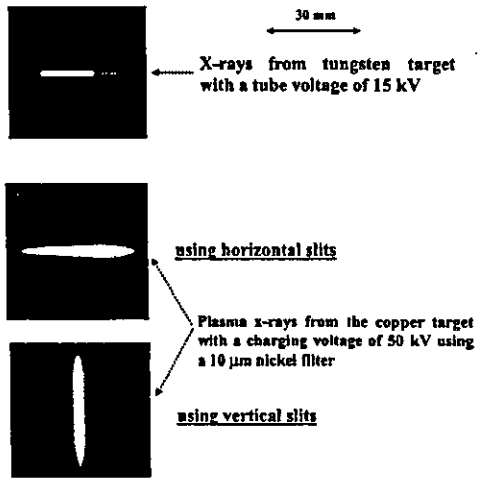


Figure 10: X-ray divergence with two lead slits.

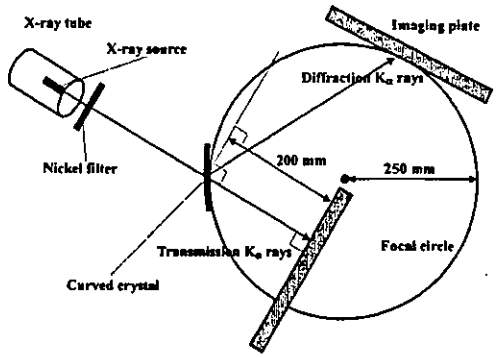


Figure 11: Experimental setup for roughly determining the rectilinear power of the characteristic $K_\alpha$ lines.

## 4. RADIOGRAPHY

The plasma radiography was performed by the CR system without using the filter, and the distance between the x-ray source and imaging plate was 1.2 m.

Firstly, rough measurements of image resolution were made using wires. Figure 12 shows radiograms of 50 μm-diameter tungsten wires coiled around a pipe and a rod made of polymethyl methacrylate with a charging voltage of 50 kV. Although the image contrast increased using the pipe, 50 μm-diameter wires could be observed.

The image of water falling into a polypropylene beaker from a glass test tube is shown in Fig. 13. This image was taken with a charging voltage of 45 kV, with the slight addition of an iodine-based contrast medium. Because the x-ray duration was about 1 μs, the stop-motion image of water could be obtained.

Figure 14 shows an angiogram of a rabbit heart; iodine-based microspheres of 20 μm in diameter were used with a charging voltage of 50 kV, and fine blood vessels of about 100 μm were visible.

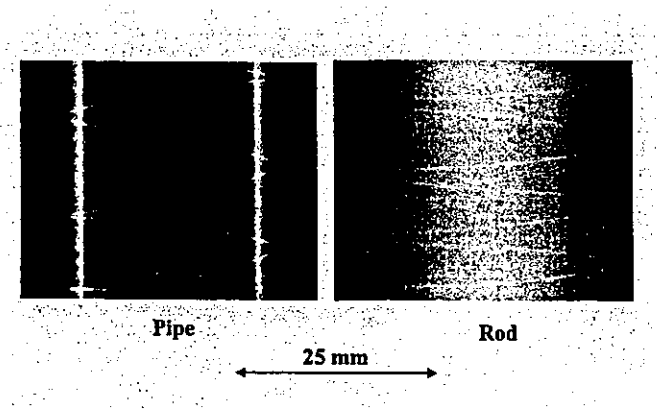


Figure 12: Radiograms of tungsten wires of 50 μm in diameter coiled around a pipe and a rod made of polymethyl methacrylate.

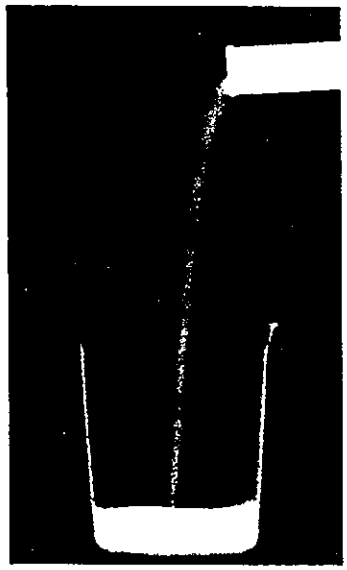

Figure 13: Radiogram of water falling into a polypropylene beaker from a glass test tube.

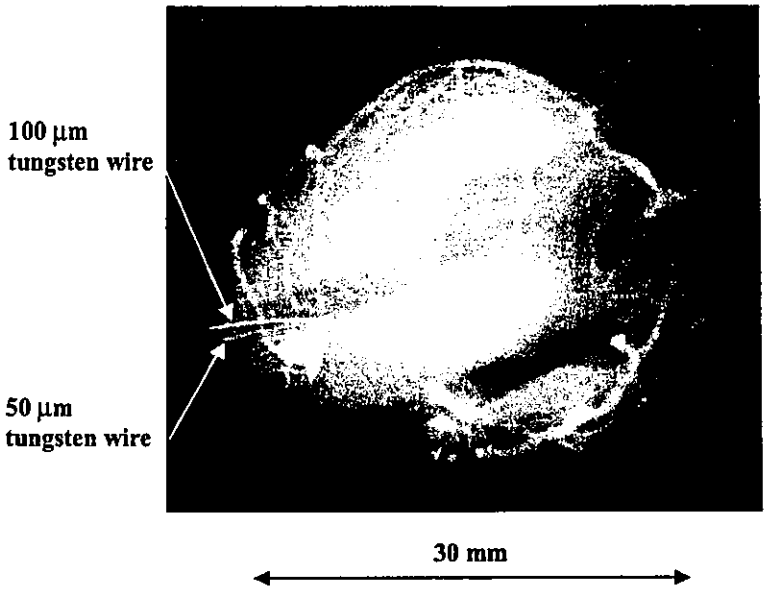


Figure 14: Angiograms of a rabbit heart.

## 5. DISCUSSION

Concerning the spectrum measurement, we obtained fairly intense and sharp $K_\alpha$ lines from a weakly ionized linear plasma x-ray source by absorbing $K_\beta$ lines using the monochromatic filter. In fact, these rays were diffused after passing through slits, and this x-ray divergence mechanism has to be solved clearly. Because the diffracting intensity rate decreases with increases in the charging voltage, the rectilinear power may be increased.

In this research, we obtained sufficient characteristic x-ray intensity per pulse for CR radiography using a monochromatic filter, and the generator produced high-count-rate monochromatic photons as compared with the synchrotron monochromatic photons. In addition, since the photon energy of characteristic x-rays can be controlled by changing the target elements, various quasi-monochromatic high-speed radiographies, such as high-contrast micro angiography[23] and parallel radiography[24,25] using an x-ray lens, will be possible.

## ACNOWLEDGMENT

This work was supported by Grants-in-Aid for Scientific Research (12670902, 13470154, and 13877114) and Advanced Medical Scientific Research from MECSST, Grants from Keiryo Research Foundation, JST (Test of Fostering Potential), NEDO, and MHLW (HLSRG, RAMT-nano-001, RHGTEFB-genome-005, and RGCD13C-1).

## REFERENCES

1. A. Mattsson, "Some characteristics of a 600 kV flash x-ray tube," *Physica Scripta*, **5**, pp. 99-102, 1972.

2. R. Germer, "X-ray flash techniques," *J. Phys. E: Sci. Instrum.*, **12**, pp. 336-350, 1979.

3. C. Cavailler, "AIRIX- a new tool for flash radiography in detonics," *SPIE*, **4183**, pp. 23-35, 2000.

4. E. Sato, H. Isobe and F. Hoshino, "High intensity flash x-ray apparatus for biomedical radiography," *Rev. Sci. Instrum.*, **57**, pp. 1399-1408, 1986.

5. E. Sato, M. Sagae, K. Takahashi, T. Oizumi, H. Ojima, K. Takayama, Y. Tamakawa, T. Yanagisawa, A. Fujiwara and K. Mitoya, "High-speed soft x-ray generators in biomedicine," *SPIE*, **2513**, pp. 649-667, 1994.

6. E. Sato, M. Sagae, K. Takahashi, A. Shikoda, T. Oizumi, H. Ojima, K. Takayama, Y. Tamakawa, T. Yanagisawa, A. Fujiwara and K. Mitoya, "Dual energy flash x-ray generator," *SPIE*, **2513**, pp. 723-735, 1994.

7. E. Sato, M. Sagae, A. Shikoda, K. Takahashi, T. Oizumi, M. Yamamoto, A. Takabe, K. Sakamaki, Y. Hayasi, H. Ojima, K. Takayama and Y. Tamakawa, "High-speed soft x-ray techniques," *SPIE*, **2869**, pp. 937-955, 1996.

8. E. Sato, S. Kimura, S. Kawasaki, H. Isobe, K. Takahashi, Y. Tamakawa and T. Yanagisawa, "Repetitive flash x-ray generator utilizing a simple diode with a new type of energy-selective function," *Rev. Sci. Instrum.*, **61**, pp. 2343-2348, 1990.

9. S. Kimura, E. Sato, M. Sagae, A. Shikoda, T. Oizumi, K. Takahashi, Y. Tamakawa and T. Yanagisawa, "Disk-cathode flash x-ray tube driven by a repetitive two-stage Marx pulser," *Med. & Biol. Eng. & Comput.*, **31**, pp. S37-S43, 1993.

10. A. Shikoda, E. Sato, M. Sagae, T. Oizumi, Y. Tamakawa and T. Yanagisawa, "Repetitive flash x-ray generator having a high-durability diode driven by a two-cable-type line pulser," *Rev. Sci. Instrum.*, **65**, pp. 850-856, 1994.

11. E. Sato, K. Takahashi, M. Sagae, S. Kimura, T. Oizumi, Y. Hayasi, Y. Tamakawa and T. Yanagisawa, "Sub-kilohertz flash x-ray generator utilizing a glass-enclosed cold-cathode triode," *Med. & Biol. Eng. & Comput.*, **32**, pp. 289-294, 1994.

12. K. Takahashi, E. Sato, M. Sagae, T. Oizumi, Y. Tamakawa and T. Yanagisawa, "Fundamental study on a long-duration flash x-ray generator with a surface-discharge triode," *Jpn. J. Appl. Phys.*, **33**, pp. 4146-4151, 1994.

13. J.J. Rocca, V. Shlyaptsev, F.G. Tomasel, O.D.Cortazar, D. Hartshorn and J.L.A. Chilla, "Demonstration of a discharge pumped table-top soft x-ray laser," *Phys. Lev. Lett.*, **73**, pp. 2192-2195, 1994.

14. J.J. Rocca, D.P. Clark, J.L.A. Chilla and V.N. Shlyaptsev, "Energy Extration and achievement of the saturation limit in a discharge-pumped table-top soft x-ray amplifier," *Phys. Lev. Lett.*, **77**, pp. 1476-1479, 1996.

15. C.D. Macchietto, B.R. Benware and J.J. Rocca, "Generation of millijoule-level soft-x-ray laser pulses at a 4-Hz repetition rate in a highly saturated tabletop capillary discharge amplifier," *Opt. Lett.*, **24**, pp. 1115-1117, 1999.

16. J.J.G. Rocca, J.L.A. Chilla, S. Sakadzic, A. Rahman, J. Filevich, E. Jankowska, E.C. Hammarsten, B.M. Luther, H.C. Kapteyn, M. Murnane and V.N. Shlyapsev, "Advances in capillary discharge soft x-ray laser research," *SPIE*, **4505**, pp. 1-6 2001.

17. E. Sato, M. Sagae, T. Ichimaru, Y. Hayasi, H. Ojima, K. Takayama, H. Ido, K. Sakamaki and Y. Tamakawa, "Tentative study on x-ray enhancement by fluorescent emission of radiation by plasma x-ray source," *SPIE*, **3771**, pp. 51-60, 1999.

18. E. Sato, Y. Suzuki, Y. Hayashi, E. Tanaka, H. Mori, T. Kawai, K. Takayama, H. Ido and Y. Tamakawa, "High-intensity quasi-monochromatic x-ray irradiation from the linear plasma target," *SPIE*, **4505**, pp. 154-164, 2001.

19. E. Sato, Y. Hayashi, E. Tanaka, H. Mori, T. Kawai, H. Obara, T. Ichimaru, K. Takayama, H. Ido, T. Usuki, K. Sato and Y. Tamakawa, "Polycapillary radiography using a quasi-x-ray laser generator," *SPIE*, **4508**, pp. 176-187, 2001.

20. E. Sato, Y. Hayasi, E. Tanaka, H. Mori, T. Kawai, T. Usuki, K. Sato, H. Obara, T. Ichimaru, K. Takayama, H. Ido and Y. Tamakawa, "Quasi-monochromatic radiography using a high-intensity quasi-x-ray laser generator," *SPIE*,

**4682**, pp. 538-548 2002.

21. E. Sato, Y. Hayasi, R. Germer, E. Tanaka, H. Mori, T. Kawai, H. Obara, T. Ichimaru, K. Takayama and H. Ido, "Intense characteristic x-ray irradiation from weakly ionized linear plasma and applications," *Jpn. J. Med. Imag. Inform. Sci.*, **20**, pp. 148-155. 2003.

22. E. Sato , K. Sato and Y. Tamakawa, "Film-less computed radiography system for high-speed Imaging," *Ann. Rep. Iwate Med. Univ. Sch. Lib. Arts and Sci.*, **35**, pp. 13-23, 2000.

ELSEVIER

Neurochemistry International 42 (2003) 261–267

NEUROCHEMISTRY International

www.elsevier.com/locate/neuint

# Effects of ketamine on exocytotic and non-exocytotic noradrenaline release

Hirotoshi Kitagawa [a,*], Toji Yamazaki [b], Tsuyoshi Akiyama [b], Hidezo Mori [b], Kenji Sunagawa [c]

[a] *Department of Anesthesia, Nagahama City Hospital, Nagahama, Japan*
[b] *Department of Cardiac Physiology, National Cardiovascular Center, Research Institute, Suita, Japan*
[c] *Department of Cardiovascular Dynamics, National Cardiovascular Center, Research Institute, Suita, Japan*

Received 29 October 2001; received in revised form 23 April 2002; accepted 2 May 2002

**Abstract**

To characterise ketamine-induced sympathomimetic action, we examined the effects of ketamine on in vivo cardiac sympathetic nerve endings function. Using adult cats given anaesthesia with pentobarbital, dialysis probes were implanted in the left ventricular myocardium and dialysate noradrenaline (NA) concentrations were measured as an indicator of NA output at the cardiac sympathetic nerve endings. Ketamine was locally administered through the dialysis probe, and dialysate NA responses were obtained in the following conditions. (1) In the resting state, ketamine (10 mM) increased dialysate NA concentration. This increase in dialysate NA was not altered by addition of ω-conotoxin GVIA (N-type $Ca^{2+}$ channel blocker) or desipramine (membrane NA uptake blocker). (2) Sympathetic activation by electrical stimulation of the stellate ganglia (ES-SG; exocytotic NA release): ES-SG caused an increase in dialysate NA, which was further augmented by addition of desipramine. During co-administration of desipramine and ketamine, dialysate NA response to ES-SG was smaller than with desipramine alone. Further, there was no significant difference in the dialysate NA response to ES-SG between ketamine and ketamine + desipramine. These data suggested that both exocytosis and NA uptake function were impaired by ketamine. (3) Non-exocytotic NA release by ouabain: ouabain caused increases in dialysate NA. These increases in dialysate NA were suppressed by ketamine, which impaired the membrane outward NA transport evoked by ouabain. We conclude that ketamine impaired exocytotic and non-exocytotic NA release. However, ketamine spontaneously evoked NA efflux that was independent of exocytosis and insensitive to NA transporter.


*Keywords:* Cat; Exocytosis; Heart; Membrane noradrenaline transport; Sympathetic nerve

## 1. Introduction

During ketamine anaesthesia, an increase in plasma noradrenaline (NA) concentration was accompanied with increased arterial pressure (Apple et al., 1979). This finding suggested that ketamine has sympathomimetic action. However, Sasao et al. (1996) demonstrated that ketamine suppressed integrated renal sympathetic nerve activity in rabbits. Furthermore, Kienbaum et al. (2000) reported that ketamine suppressed sympathetic discharge to muscle but augmented plasma NA concentrations in man. Conflicting results of the effect of ketamine on sympathetic nerve activity and neurotransmitter release may be explained by ketamine-induced abnormalities at the sympathetic nerve endings. Recently, several studies have demonstrated that ketamine inhibits neuronal NA uptake in cultured adrenal medullary cells (Hara et al., 1998) and isolated ventricular myocardium (Cook et al., 1992). Alternatively, ketamine was reported to induce non-exocytotic NA release at the sympathetic nerve endings in the isolated perfused heart (Saegusa et al., 1986). Both findings can explain an increase in plasma NA in spite of reduced sympathetic nerve activity. However, it is still uncertain which effect plays a critical role at in vivo sympathetic nerve endings.

We focus here on the effects of ketamine on NA kinetics at sympathetic nerve endings. In the previous study, we reported that dialysis technique makes it possible to assess NA release and NA uptake at in vivo cardiac sympathetic nerve endings (Yamazaki et al., 1997). Furthermore, with pharmacological agents, it is possible to dissociate exocytotic and non-exocytotic NA release at the sympathetic nerve endings (Yahagi et al., 1998; Yamazaki et al., 1997). Therefore, using cardiac dialysis technique in the in vivo heart

* Corresponding author. Present address: Department of Anesthesiology, Shiga University of Medical Science, Otsu, Shiga 520-2192, Japan. Tel.: +81-77-548-2281; fax: +81-77-548-2781.
*E-mail address:* hirotosi@belle.shiga-med.ac.jp (H. Kitagawa).

0197-0186/03/$ – see front matter 
PII: S0197-0186(02)00090-6

(Akiyama et al., 1991), the present study was undertaken to examine to what extent local administration of ketamine modulates the neuronal NA release and uptake at the cardiac sympathetic nerve endings. Further, we examined whether ketamine evokes non-exocytotic NA release and how ketamine modulates the non-exocytotic NA release induced by ouabain (Vizi, 1978).

## 2. Methods

### 2.1. Animal preparation

Animal care and all procedures were conducted in strict accordance with the guiding principles of the Physiological Society of Japan. Thirty-five adult cats of either sex (2.1–4.1 kg) were used in this study.

Anaesthesia was induced with pentobarbital (30–35 mg/kg i.p.). After tracheal intubation, anaesthesia was maintained with an intravenous infusion of pentobarbital (1–2 mg/kg/h). The animals were immobilised with pancuronium (0.5 mg/h i.v.) and ventilated with room air mixed with oxygen. The tidal volume and respiratory rate were adjusted to maintain arterial carbon dioxide tension. Oesophageal temperature was monitored and kept at 37 °C by means of a heating pad and lamp. The electrocardiogram was recorded with surface electrodes, and arterial pressure and heart rate were simultaneously monitored.

The fifth or sixth rib on the left side was partially removed to expose the heart. One or two dialysis probes were implanted in the left ventricle free wall of the beating heart using a fine guiding needle. Heparin sodium (100 U/kg) was intravenously administered to prevent blood coagulation, and a maintenance dose was given every 2 h. In the case of nerve stimulation, the second rib on both sides was removed, and the regions of the stellate ganglia were exposed through the intercostal space. Cardiac sympathetic nerves were bilaterally transected at the stellate ganglia, and distal ends were stimulated using a nerve stimulator in protocol 2.

### 2.2. In vivo dialysis technique

We measured dialysate NA concentrations as indices of myocardial interstitial NA concentrations. The material and properties are described elsewhere (Akiyama et al., 1991; Yamazaki et al., 1995). In brief, a dialysis fibre (13 mm length, 0.31 mm o.d., and 0.2 mm i.d.; PAN-1200, 50 000 molecular weight cut-off, Asahi Chemical, Tokyo, Japan) was glued at both ends to a polyethylene tube (20 cm length, 0.5 mm o.d., and 0.2 mm i.d.). The dialysis probes were perfused with Ringer solution at a rate of 10 μl/min using a microinjection pump. To allow the NA concentrations to reach a steady state, the dialysate sampling was started at 120 min after implantation of the dialysis probe. Taking into account the dead space volume between the dialysis membrane and sample tube, we started dialysate sampling. Sampling periods were 4 min in duration (one sampling volume = 40 μl). Each sample was collected in a microtube containing 4 μl of 0.1 N HCl to prevent amine oxidation.

### 2.3. Experimental protocols

#### 2.3.1. Preliminary studies: dose dependent ketamine-induced dialysate NA responses

We examined the effects of varying doses (100 μM, 1 mM, 10 mM) of ketamine on dialysate NA concentrations in separate cats. The dialysis probe was perfused with Ringer solution containing ketamine and dialysate samples obtained 60 min after starting local administration of ketamine. Ketamine at 10 mM increased dialysate NA concentrations (Fig. 1). This dose was chosen for the following experiments.

#### 2.3.2. Protocol 1: influence of neuronal blocking agents on dialysate NA response evoked by ketamine

The myocardial interstitial NA concentration is mainly determined by NA release and NA uptake at surrounding cardiac sympathetic nerve endings (Eisenhofer et al., 1991; Kitagawa et al., 1998). To test the hypothesis that the ketamine-induced dialysate NA response was mainly

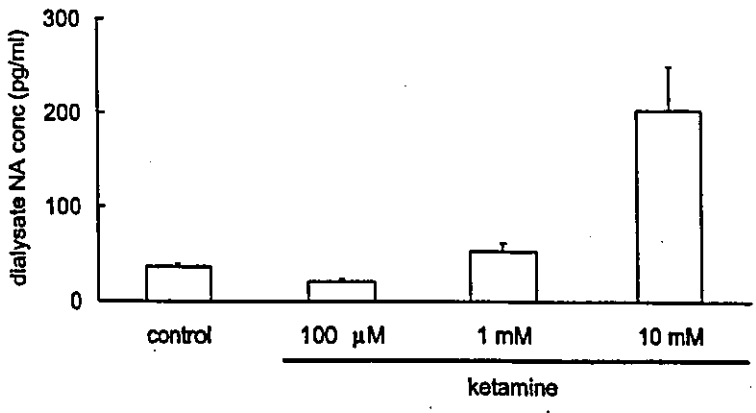


Fig. 1. Effect of varying doses (100 μM, 1 mM, 10 mM) of ketamine on dialysate NA concentrations. Ketamine (10 mM) was locally administered through the dialysis probe and increased dialysate NA concentrations. Values are means ± S.E. ($n = 3$).

involved in exocytotic NA release or impaired NA uptake at the cardiac sympathetic nerve endings, ketamine-induced NA responses were compared with and without either ω-conotoxin GVIA (N-type $Ca^{2+}$ channel blocker: 10 μg/kg i.v.) or desipramine (membrane NA uptake blocker: 100 μM). Furthermore, to test the effect of ketamine on NA release including exocytotis and non-exocytosis (carrier-mediated outward NA transport), the ketamine-induced dialysate NA response was measured with the pretreatment of both ω-conotoxin GVIA and desipramine. Neuropharmacological agents were administered in a separate group of cats. The ketamine-induced dialysate NA response was expressed as the change in dialysate NA from basal concentration.

#### 2.3.3. Protocol 2: influences of ketamine on nerve stimulation-induced dialysate NA responses

To test the modulatory effect of ketamine on exocytotic NA release from in vivo cardiac sympathetic nerve endings, the nerve stimulation-induced dialysate NA responses were measured. Bilateral distal ends of transected stellate ganglia were stimulated consecutively at 5 Hz (10 V, 1 ms in duration) and the dialysate was sampled before and during 4 min nerve stimulation. Dialysate samples were obtained in the presence and absence of ketamine. Furthermore, to test the effect of ketamine on neuronal NA uptake, we compared the nerve stimulation-induced NA responses in the presence and absence of ketamine with desipramine (100 μM) pretreatment. Neuropharmacological agents were administered in a separate group of cats. The ketamine-induced dialysate NA response was expressed as the change in dialysate NA from basal concentration.

#### 2.3.4. Protocol 3: influence of ketamine on ouabain-induced dialysate NA response

To test the modulatory effect of ketamine on non-exocytotic NA release, ouabain-induced NA responses were measured. The previous studies demonstrated that locally applied ouabain caused carrier-mediated outward NA transport (non-exocytotic NA release) from sympathetic nerve endings (Maekawa et al., 2001; Reines et al., 2001; Sumiya et al., 2001; Sweadner, 1985; Vizi, 1978; Yamazaki et al., 1999). Ouabain at 100 μM was locally administered through the dialysis probe, and the dialysate was sampled at 10 min intervals during 60 min administration. Ouabain-induced NA responses were compared with and without pretreatment of ketamine.

The experimental animals were killed at the end of the experiments with an overdose of pentobarbital sodium. We then verified the position of the dialysis probe in the middle layer of the left ventricular myocardium.

### 2.4. Analytical procedures

Dialysate NA concentrations were measured by high-performance liquid chromatography with electrochemical detection (Eicom, Kyoto, Japan). The chromatographic column consists of a gird column (CA-ODS, 5 mm × 4 mm i.d., Eicom) and analytic reversed-phase column (Eicompack CA-5ODS, 150 mm × 2.1 mm i.d., Eicom). An alumina procedure was performed to remove the interfering compounds from the dialysate (Akiyama et al., 1991). The amperometric detector was operated at 0.40 V versus an Ag/AgCl reference electrode. In the mobile phase, 0.1 M phosphate buffer (pH 6.1) was used with methanol, disodium-EDTA and 1-octanesulfonic acid sodium salt (Yamazaki et al., 1995). The pump flow rate was 0.25 ml/min. The absolute detection limit of NA was 0.1 pg/50 μl injection (signal-to-noise ratio = 3).

### 2.5. Statistical analysis

One-way analysis variance was applied to analyse differences (Winer, 1971). When statistical significance was detected, the tukey procedure was applied. Unpaired *t*-test was performed to compare the ouabain-induced response of dialysate NA concentrations with and without ketamine. Statistical significance was defined as $P < 0.05$. Values are presented as means ± standard error.

## 3. Results

### 3.1. Protocol 1: influence of neuronal blocking agents on dialysate NA response evoked by ketamine

Local administration of ketamine did not affect the changes in systemic hemodynamics or ECG. Ketamine increased dialysate NA concentrations to 137 ± 11 pg/ml at 60 min of ketamine administration. This high concentration was maintained during 120 min administration. The pretreatment with ω-conotoxin GVIA, desipramine and combination of ω-conotoxin GVIA and desipramine altered basal dialysate NA concentrations (Table 1). However, there were no significant differences in ketamine-induced NA responses among these groups (Fig. 2).

Table 1
Basal dialysate NA concentrations

| | Dialysate NA concentrations (pg/ml) |
|---|---|
| Protocol 1 | |
| Vehicle | 37 ± 3 |
| ω-Conotoxin GVIA | 24 ± 3 |
| Desipramine | 91 ± 9 |
| ω-Conotoxin GVIA + desipramine | 69 ± 9 |
| Protocol 2 (after transection of stellate ganglia) | |
| Vehicle | 18 ± 5 |
| Desipramine | 74 ± 6 |
| Ketamine | 135 ± 19 |
| Ketamine + desipramine | 183 ± 39 |

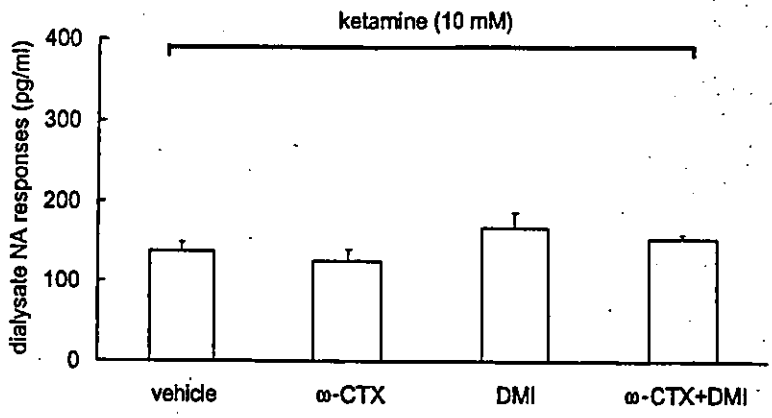


Fig. 2. Ketamine (10 mM)-induced dialysate NA responses in various conditions. Pretreatment with ω-conotoxin GVIA (ω-CTX) and/or desipramine (DMI) did not alter dialysate NA response. Values are means ± S.E. ($n = 5$).

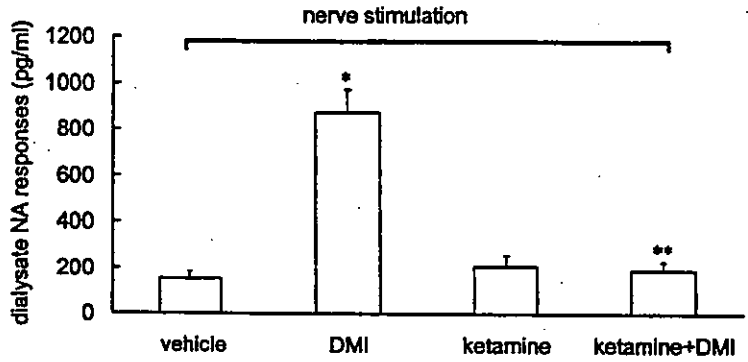


Fig. 3. Effect of ketamine (10 mM) and desipramine (DMI) (100 μM) on dialysate NA responses to electrical stimulation of stellate ganglia (5 Hz, 10 V). Values are means ± S.E. ($n = 6$). $^{*}P < 0.05$ vs. value in vehicle group; $^{**}P < 0.05$ vs. value in desipramine alone group.

### 3.2. *Protocol 2: influences of ketamine on nerve stimulation-induced dialysate NA responses*

Electrical stimulation of the stellate ganglia increased dialysate NA concentration to 150 ± 31 pg/ml (Fig. 3). The stimulation-induced NA response was augmented by administration of desipramine. Ketamine pretreatment caused an increase in basal dialysate NA concentrations (Table 1), but the nerve stimulation-induced NA response was not altered in comparison with the vehicle group. Furthermore, with pretreatment of ketamine and desipramine, nerve stimulation-induced NA responses were not altered in comparison with ketamine alone but suppressed in comparison with the desipramine group. These data suggested

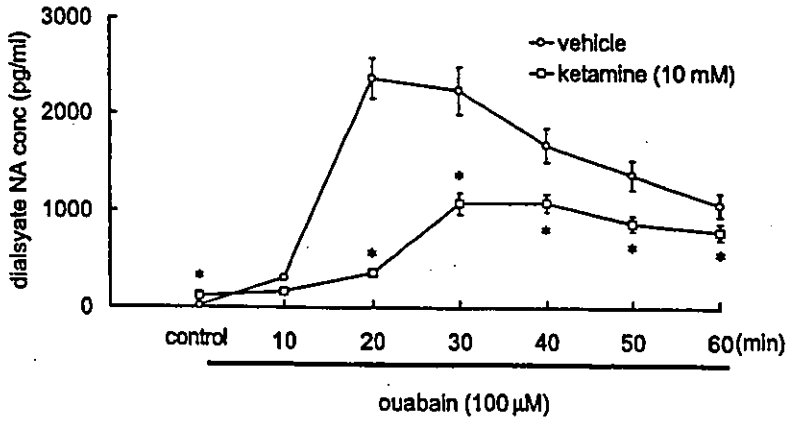


Fig. 4. Time course of dialysate NA concentrations during local administration of ouabain (100 μM) with and without pretreatment of ketamine. Values are means ± S.E. ($n = 6$). $^{*}P < 0.05$ vs. concurrent value in vehicle group.

that ketamine suppressed both exocytotic NA release and NA uptake evoked by the electrical stimulation of cardiac sympathetic nerves.

### 3.3. Protocol 3: influence of ketamine on ouabain-induced dialysate NA response

Fig. 4 presents the time course of the dialysate NA concentrations during local administration of ouabain (100 μM). In the vehicle group, dialysate NA concentration increased significantly to 2371 ± 215 pg/ml at 20 min during ouabain administration. With the addition of ketamine, ouabain caused increases in dialysate NA. In comparison with the vehicle group, ketamine suppressed the ouabain-induced NA response at 20–60 min during ouabain administration.

## 4. Discussion

Our result demonstrates that, in an in vivo cat heart, locally applied 10 mM ketamine caused a brisk increase in dialysate NA concentration. This NA increment was not augmented by addition of desipramine. In vitro studies suggested that ketamine inhibited neuronal NA uptake at the sympathetic nerve endings (Cook et al., 1992). If ketamine shares the inhibitory effect of neuronal NA uptake with desipramine via the same binding site (Hara et al., 1998), the absence of any effect of desipramine on ketamine-induced NA efflux may be explained in part by this mechanism. If this is the case, exocytotic NA release was accompanied by subsequent NA uptake inhibition, and ketamine-induced NA efflux could be reduced by addition of ω-conotoxin GVIA. However, ketamine-induced NA efflux was not reduced by pretreatment with ω-conotoxin GVIA. This result indicates that ketamine-induced NA efflux was independent of N-type $Ca^{2+}$ channel opening coupled to exocytosis, and participation of ketamine on the inhibition of neuronal NA uptake may be ruled out. Furthermore, carrier-mediated NA transport was not involved in the change of dialysate NA evoked by ketamine because desipramine blocks carrier-mediated NA transport bi-directionally (Akiyama and Yamazaki, 1999; Yamazaki et al., 1997). Alternatively, ketamine may exert a dual action via exocytosis or neuronal NA transport. Then, the addition of desipramine or ω-conotoxin GVIA only may inhibit each action and residual action may cause a redundant effect on ketamine-induced NA efflux. Pretreatment with ω-conotoxin GVIA and desipramine did not alter ketamine-induced NA efflux. Thus, ketamine-induced NA efflux was independent of N-type $Ca^{2+}$ channel coupled to exocytosis and insensitive to carrier-mediated neuronal NA transport, and might be due to the passive diffusion from the axoplasmic site.

Electrical stimulation of the stellate ganglia caused an increase in dialysate NA concentrations, which was blocked by addition of ω-conotoxin GVIA (Yamazaki et al., 1997). Although ketamine evoked spontaneous NA efflux, nerve-stimulation further facilitated the dialysate NA concentrations by exocytosis. There was no significant difference in the NA response evoked by nerve stimulation between the vehicle and ketamine groups. This result indicates that ketamine did not appear to affect the exocytotic NA release evoked by nerve stimulation. However, with the addition of desipramine and ketamine, the nerve stimulation-induced NA response was suppressed in comparison with the desipramine group. During pretreatment with a neuronal NA uptake blocker such as desipramine, the nerve stimulation-induced dialysate NA response expresses the total amount of exocytotic NA release because subsequent neuronal NA uptake is blocked with desipramine (Eisenhofer et al., 1991; Yamazaki et al., 1997). Therefore, these results indicate that ketamine caused suppression of the exocytotic NA release evoked by electrical stimulation of sympathetic nerves. Furthermore, desipramine did not affect the NA response evoked by nerve stimulation during ketamine administration. This result indicates that ketamine may share the inhibition of neuronal NA uptake with desipramine via the same binding site (Hara et al., 1998). These data suggested that ketamine suppressed exocytotic NA release and NA uptake evoked by the electrical stimulation of the stellate ganglia. The impairment of NA uptake may mask inhibitory action of ketamine on NA release. Only either inhibition of NA release or NA transport did not interpret overall data on the nerve-stimulation.

The suppressive effect of ketamine on exocytotic NA release might be related to its action on the inhibition of $Na^+$ channel at the surrounding sympathetic axon (Allaoua and Chicheportiche, 1989; Brau et al., 1997). If so, our results (protocol 1 and 2) were consistent with the conflicting results of the effect of ketamine on sympathetic nerve activity and neurotransmitter release in the clinical setting (Apple et al., 1979; Kienbaum et al., 2000). Alternatively, during ketamine administration, the amount of NA efflux from axoplasmic site may be greater that that of membrane NA uptake. Thus, opposing NA efflux may underestimate the amount of neuronal NA uptake. Furthermore, on the result of protocol 1, the lack of effect of ω-conotoxin GVIA and desipramine can be explained in part by this suppression of exocytosis and NA uptake.

Only either inhibition of NA release or NA transport did not interpret overall data on the nerve-stimulation. Ouabain evoked a brisk increase in dialysate NA by inhibition of $Na^+$-$K^+$ ATPase. Inhibition of $Na^+$-$K^+$ ATPase caused accumulation of intracellular $Na^+$ which could carry NA out of the axoplasma with NA transporter (Sweadner, 1985; Yamazaki et al., 1999). Ketamine suppressed the increment in dialysate NA response evoked by ouabain. This result indicates that ketamine evoked the inhibition of carrier-mediated NA transport. This action induced by ketamine is similar to that induced by desipramine, with the binding sites possibly the same. Taken together (protocol 2 and 3), our data suggest that ketamine blocks both normal and reverse NA transport.

Although local administration of ketamine acted by releasing NA that was independent of ω-conotoxin GVIA and insensitive to desipramine, ketamine suppressed both the exocytotic NA release evoked by nerve stimulation and non-exocytotic NA release evoked by pharmacological intervention (ouabain). Desipramine insensitive and ω-conotoxin GVIA resistant NA efflux was observed under co-administration of a vesicle NA transport inhibitor (reserpine) and a monoamine oxidase inhibitor (pargyline) (Yamazaki et al., 1997). Co-administration of these agents leads to the mobilization of NA from stored NA vesicle to axoplasma and the accumulation of NA in the axoplasmic site. Ketamine also may displace NA towards the axoplasma and extraneuronal spaces. A similar mechanism was proposed for tyramine-induced NA efflux (Bönisch and Trendelenburg, 1988; Takauchi et al., 2000). However, in the case of tyramine, the neuronal NA transport carrier that transported tyramine into the axoplasma induced the outward transport of NA from axoplasmic site. On the other hand, the neuronal NA transport carrier did not transport ketamine, and NA efflux seems to be derived via passive diffusion, which is an outward chemical gradient for NA. Furthermore, the mobilization of NA from the stored vesicle to the axoplasmic site may lead to exhaustion of NA at the stored NA vesicle. Consequently, exocytotic NA release evoked by nerve stimulation was suppressed. In two different stimulations (perturbation induced exocytotic and non-exocytotic NA release), ketamine seems to inhibit carrier-mediated NA transport bi-directionally. This result may be consistent with the finding that ketamine-induced NA efflux was due to passive diffusion rather than an accelerated exchange diffusion mechanism.

### 4.1. Methodological considerations

There are several limitations to the present study. First, we investigated myocardial NA concentrations in cats anaesthetised with pentobarbital sodium. Because this barbiturate anaesthesia affects the autonomic nervous system (Hirota et al., 2000), the results might have altered if non-barbiturate anaesthesia or no anaesthesia had been used. Pentobarbital anaesthesia might interact with locally applied ketamine on NA kinetics.

Second, we administered ketamine as a racemate through the dialysate probes. Recently, ketamine has been reported to consist of two isomers, S(+)- and R(−)-ketamine (Hancock and Stamford, 1999; Nishimura and Sato, 1999). Stereospecific effects of ketamine on monoamine kinetic at the nerve ending have been discussed. Complicated results may be dissociated with stereoselectivity. Further studies are clearly required to elucidate the effect of selective isomer on the NA kinetics.

Local administration of ketamine spontaneously evoked NA efflux that was independent of ω-conotoxin GVIA and insensitive to desipramine. Further, ketamine suppressed exocytotic NA release evoked by nerve stimulation and non-exocytotic NA release evoked by pharmacological intervention (ouabain). These results may be explained in part by the suppression by ketamine of sympathetic discharge but augmentation of plasma NA concentrations. Furthermore, these complicated effects of ketamine may gain relevance during ketamine-induced neuroprotection in ischemic brain.

## References


Akiyama, T., Yamazaki, T., 1999. Norepinephrine release from cardiac sympathetic nerve endings in the in vivo ischemic region. J. Cardiovasc. Pharmocol. 34 (Suppl. 4), S11–14.

Akiyama, T., Yamazaki, T., Ninomiya, I., 1991. In vivo monitoring of myocardial interstitial norepinephrine by dialysis technique. Am. J. Physiol. 261, H1643–H1647.

Allaoua, H., Chicheportiche, R., 1989. Anaesthetic properties of phencyclidine (PCP) and analogues may be related to their interaction with $Na^+$ channels. Eur. J. Pharmacol. 25, 327–335.

Apple, E., Dudziak, R., Palm, D., Wnuk, A., 1979. Sympathoneuronal and sympathoadrenal activation during ketamine anesthesia. Eur. J. Clin. Pharmacol. 16, 91–95.

Bönisch, H., Trendelenburg, U., 1988. Mechanism of action of indirectly acting sympathomimetic amines. In: Trendelenburg, U., Weiner, N. (Eds.), Handbook of Experimental Pharmacology, Vol. 90/1. Catecholamine 1, Springer, Berlin, pp. 246–277.

Brau, M.E., Sander, F., Vogel, W., Hempelmann, G., 1997. Blocking mechanisms of ketamine and its enantiomers in enzymatically demyelinated peripheral nerve as revealed by single-channel experiments. Anesthesiology 86, 394–404.

Cook, D.J., Housmans, P.R., Rorie, D.K., 1992. Effect of ketamine HCL on norepinephrine disposition in isolated ferret ventricular myocardium. J. Pharmacol. Exp. Ther. 261, 101–107.

Eisenhofer, G., Smolich, J.J., Cox, H.S., Esler, M.D., 1991. Neuronal reuptake of norepinephrine and production of dihydroxyphenylglycol by cardiac sympathetic nerves in the anesthetized dogs. Circulation 84, 1354–1363.

Hancock, P.J., Stamford, J.A., 1999. Stereospecific effects of ketamine on dopamine efflux and uptake in the rat nucleus accumbens. Br. J. Anaesth. 82, 603–608.

Hara, K., Yanagihara, N., Minami, K., Ueno, S., Toyohira, Y., Sata, T., Kawamura, M., Bruss, M., Bonish, H., Shigematsu, A., Izumi, F., 1998. Ketamine interacts with the noradrenaline transporter at a site partly overlapping the desipramine binding site. Naunyn Schmiedebergs Arch. Pharmacol. 358, 328–333.

Hirota, K., Kudo, M., Kudo, T., Kitayama, M., Kushikata, T., Lambert, D.G., Matsuki, A., 2000. Barbiturates inhibit K(+)-evoked noradrenaline and dopamine release from rat striatal slices—involvement of voltage sensitive Ca(2+) channels. Neurosci. Lett. 291, 175–178.

Kienbaum, P., Heuter, T., Michel, M.C., Peters, J., 2000. Racemic ketamine decreases muscle sympathetic activity but maintains the neuronal response to hypotensive challenges in humans. Anesthesiology 92, 94–101.

Kitagawa, H., Akiyama, T., Yamazaki, T., 1998. Myocardial interstitial noradrenaline monitoring during occlusion of inferior vena cava in cats. Acta Physiol. Scand. 163, 173–179.

Nishimura, M., Sato, K., 1999. Ketamine stereoselectively inhibits rat dopamine transporter. Neurosci. Lett. 272, 131–134.

Maekawa, M., Murayama, T., Nomura, Y., 2001. Involvement of noradrenaline transports in S-nitrosocysteine-stimulated noradrenaline release from rat brain slices: existence of functional Na(+)-independent transport activity. Neurochem. Int. 38, 323–331.

Reines, A., Pena, C., Arnaiz, G., 2001. [$^3$H]Dizocilpine binding to *N*-methyl-D-asparate (NMDA) receptor is modulated by an endogenous $Na^+$, $K^+$-ATPase inhibitor. Comparison with ouabain. Neurochem. Int. 39, 301–310.

Saegusa, K., Furukawa, Y., Ogiwara, Y., Chiba, S., 1986. Pharmacologic analysis of ketamine-induced cardiac actions in isolated, blood-perfused canine atria. J. Cardiovasc. Pharmacol. 8, 414–419.

Sasao, J., Taneyama, C., Kohno, N., Goto, H., 1996. The effects of ketamine on renal sympathetic nerve activity and phrenic nerve activity in rabbits (with vagotomy) with and without afferent inputs from peripheral receptors. Anesth. Analg. 82, 362–367.

Sumiya, Y., Torigoe, K., Gerevich, Z., Kofalvi, A., Vizi, E.S., 2001. Excessive release of [$^3$H]noradrenaline by veratridine and ischemeia in spinal cord. Neurochem. Int. 39, 59–63.

Sweadner, K.J., 1985. Ouabain-evoked norepinephrine release from intact rat sympatheic neurons: evidence for carrier-mediated release. J. Neurosci. 9, 2397–2406.

Takauchi, Y., Yamazaki, T., Akiyama, T., 2000. Tyramine-induced endogenous noradrenaline efflux from in situ cardiac sympathetic nerve ending in cats. Acta Physiol. Scand. 168, 287–293.

Vizi, E.S., 1978. $Na^+$, $K^+$ activated adnosinetriphosphate as a trigger in transmitter release. Neuroscience 3, 367–384.

Winer, B.J., 1971. Statistical Principles in Experimental Design, 2nd Edition. McGraw-Hill, New York.

Yahagi, N., Akiyama, T., Yamazaki, T., 1998. Effects of ω-conotoxin GVIA on cardiac sympathetic nerve function. J. Auton. Nerv. Syst. 68, 43–48.

Yamazaki, T., Akiyama, T., Shindo, T., 1995. Routine high-performance liquid chromatographic determination of myocardial interstitial norepinephrine. J. Chromatogr. B Biomed. Appl. 670, 328–331.

Yamazaki, T., Akiyama, T., Kitagawa, H., Takauchi, Y., Kawada, T., Sunagawa, K., 1997. A new, concise dialysis approach to assessment of cardiac sympathetic nerve terminal abnormalities. Am. J. Physiol. 272, H1182–H1187.

Yamazaki, T., Kawada, T., Akiyama, T., Kitagawa, H., Takauchi, Y., Yahagi, N., Sunagawa, K., 1997. ω-Conotoxin GVIA and desipramine insensitive norepinephrine efflux from cardiac sympathetic nerve terminal. Brain Res. 761, 329–332.

Yamazaki, T., Akiyama, T., Kawada, T., 1999. Effects of ouabain on in situ cardiac sympathetic nerve endings. Neurochem. Int. 35, 439–445.

Journal of the American College of Cardiology
© 2003 by the American College of Cardiology Foundation
Published by Elsevier Science Inc.

Vol. 41, No. 6, 2003
ISSN 0735-1097/03/$30.00
doi:10.1016/S0735-1097(02)03007-3

# Biodegradable Gelatin Hydrogel Potentiates the Angiogenic Effect of Fibroblast Growth Factor 4 Plasmid in Rabbit Hindlimb Ischemia

Hirofumi Kasahara, MD,* Etsuro Tanaka, MD, PhD,†§ Naoto Fukuyama, MD, PhD,†§ Eriko Sato, MD,* Hiromi Sakamoto, PhD,‖ Yasuhiko Tabata, PhD,¶ Kiyoshi Ando, MD, PhD,‡§ Harukazu Iseki, MD, PhD,‡ Yoshiro Shinozaki, BS,† Koji Kimura, MD,* Eriko Kuwabara, MD,* Shirosaku Koide, MD, PhD,* Hiroe Nakazawa, MD, PhD,† Hidezo Mori, MD, PhD#

*Isehara, Tokyo, Kyoto, and Suita, Japan*

**OBJECTIVES** We investigated the potentiation of gene therapy using fibroblast growth factor 4 (FGF4)-gene by combining plasmid deoxyribonucleic acid (DNA) with biodegradable gelatin hydrogel (GHG).

**BACKGROUND** Virus vectors transfer genes efficiently but are biohazardous, whereas naked DNA is safer but less efficient. Deoxyribonucleic acid charges negatively; GHG has a positively charged structure and is biodegradable and implantable; FGF4 has an angiogenic ability.

**METHODS** The GHG-DNA complex was injected into the hindlimb muscle (63 mice and 55 rabbits). Gene degradation was evaluated by using $^{125}$I-labeled GHG-DNA complex in mice. Transfection efficiency was evaluated with reverse-transcription nested polymerase chain reaction and X-Gal histostaining. The therapeutic effects of GHG-FGF4-gene complex (GHG-FGF4) were evaluated in rabbits with hindlimb ischemia.

**RESULTS** Gelatin hydrogel maintained plasmid in its structure, extending gene degradation temporally until 28 days after intramuscular delivery, and improving transfection efficiency. Four weeks after gene transfer, hindlimb muscle necrosis was ameliorated more markedly in the GHG-FGF4 group than in the naked FGF4-gene and GHG-beta-galactosidase (control) groups ($p < 0.05$, Kruskal-Wallis test). Synchrotron radiation microangiography (spatial resolution, 20 μm) and flow determination with microspheres confirmed significant vascular responsiveness to adenosine administration in the GHG-FGF4 group, but not in the naked FGF4-gene and the control.

**CONCLUSIONS** The GHG-FGF4 complex promoted angiogenesis and blood flow regulation of the newly developed vessels possibly by extending gene degradation and improving transfection efficiency without the biohazard associated with viral vectors. (J Am Coll Cardiol 2003;41: 1056–62) © 2003 by the American College of Cardiology Foundation

Angiogenic gene therapy using growth factors is widely studied to treat ischemic heart disease and severe limb ischemia (1,2). Of the two major methods of gene transfer, the use of virus vectors is efficient but biohazardous (3,4), while naked deoxyribonucleic acid (DNA) is safer, but less efficient (5). A highly efficient and safe drug delivery system without using a virus vector is needed for gene therapy in humans. We developed a new hydrogel consisting of amino acids, being biodegradable and, therefore, implantable, from gelatin (6). Hydrogel has been used to improve transfection efficiency in a hydrogel-coated balloon catheter (7). However, this hydrogel was not implantable because it consisted of carbohydrate and was not biodegradable. The purpose of the present study is to assess whether biodegradable gelatin hydrogel (GHG) improves the efficacy of gene therapy with the fibroblast growth factor 4 (FGF4)/hst1 gene; FGF4 is a growth factor discovered in human gastric cancer (8) and has a secretion signal domain (9). Its angiogenic ability has been confirmed both in vitro and in vivo (10).

## METHODS

**Experimental animals.** All animal experiments were performed in accordance under the Guidelines of Tokai University School of Medicine on Animal Use, which conform to the National Institute of Health (NIH) Guide for the Care and Use of Laboratory Animals, DHEW publication No. (NIH) 86-23, revised 1985, Offices of Science and Health Reports, DRR/NIH, Bethesda, Maryland. Fifty-five Japanese white rabbits weighting 2.45 to 2.85 kg (Nihon Nosan Co., Tokyo, Japan) of both genders were used. The animals were anesthetized by intravenous injection of sodium pentobarbital (40 mg/kg), and hindlimb ischemia was created by the method of Takeshita et al. (11). Sixty-three

From the Departments of *Cardiovascular Surgery, †Physiology, ‡Internal Medicine, and §Research Center for Genetic Engineering and Cell Transplantation, Tokai University School of Medicine, Isehara, Japan; ‖Genetics Division, National Cancer Center Research Institute, Tokyo, Japan; ¶Research Center for Biomedical Engineering, Kyoto University, Kyoto, Japan; #Department of Cardiac Physiology, National Cardiovascular Center Research Institute, Suita, Japan. Supported by Grants-in-Aid for Scientific Research (13470154, 13470381, 13877114, 14657460, 14657461) from the MECSST; New Energy and Industrial Technology Development Organization; The Science Frontier Program of MESSC; The Research Grants for Cardiovascular Disease (H13C-1) and for Cancer Research (9-3, 10Shi-1) from the MHLW; HLSRG-H14nano001&genom005; the Promotion of Fundamental Studies in Health Science of the Organization for Pharmaceutical Safety and Research of Japan.

Manuscript received December 30, 2001; revised manuscript received July 2, 2002, accepted November 5, 2002.

**Abbreviations and Acronyms**

| | |
|---|---|
| ANOVA | = analysis of variance |
| cDNA | = complementary deoxyribonucleic acid |
| DNA | = deoxyribonucleic acid |
| FGF4 | = fibroblast growth factor 4 |
| GHG | = gelatin hydrogel |
| lacZ | = beta-galactosidase |
| NIH | = National Institute of Health |
| PBS | = phosphate-buffered saline |
| pI | = isoelectric point |
| RNA | = ribonucleic acid |
| RT-nested PCR | = reverse transcription-nested polymerase chain reaction |

mice (male ddY mice, six to seven weeks old, Shizuoka Animal Center, Shizuoka, Japan) were also used.

**Preparation of GHG-DNA complex.** DNA encoding FGF4, beta-galactosidase (lacZ) with the cytomegalovirus enhancer-chicken β-actin hybrid promoter comprising a cytomegalovirus enhancer, and chicken beta-actin promoter were constructed (12); GHG was prepared from bovine bone (6). The GHG used in this study was characterized by a spheroid shape with a diameter of approximately 200 μm, water content of 95%, and an isoelectric point (pI) of 11 after swelling in water, without special statement.

The efficiency of incorporation of DNA into positively and negatively charged GHG was evaluated. Dried GHG (4 mg, pI 11 or 5) was added to lacZ DNA solution (500 μg/100 μl in phosphate-buffered saline [PBS], pH 7.4), mixed with a vortex mixer for 5 s, and allowed to stand at 37°C; the solution immediately settled. The absorbance (260 nm) of the supernatant was measured. In a sham control experiment, GHG was added to pure PBS solution. Positively charged GHG (pI 11) was immediately impregnated with naked DNA, and was stable at pH 7.4 for at least 120 h, whereas the negatively charged one (pI 5) was not.

**Experimental protocols.** PROTOCOL 1: DNA DEGRADATION AND THE IMPROVEMENT OF TRANSFECTION EFFICIENCY BY GHG. To examine the temporal extension of gene degradation by GHG, the decay sequence of $^{125}$I-labeled DNA impregnated into unlabeled GHG, $^{125}$I-labeled GHG, and $^{125}$I-labeled DNA solution was compared (63 mice). Plasmid DNA and GHG were radioiodinated with $^{125}$I, with TICl3 and Bolton and Hunter reagent (Amersham Pharmacia Biotech Ltd., Buckinghamshire, United Kingdom) (13), respectively. To impregnate GHG with DNA, dried GHG (2 mg) was added to 100 μl of naked lacZ solution (50 μg/100 μl in PBS), mixed for 5 s, and allowed to stand at 37°C for 2 h. Each complex was injected into the hindlimb muscle. On days 1, 3, 5, 7, 14, 21, or 28, the muscle was collected, and radioactivity was measured with a gamma counter (ARC-301B, Aloka Co., Ltd., Tokyo, Japan) in three mice each.

The following experiment was performed in 16 rabbits to assess spatial potentiation of gene expression by GHG. Intramuscular gene transfer was performed 10 days after modeling hindlimb ischemia. The DNA solution (FGF4-gene or lacZ 500 μg/100 μl PBS) mixed with GHG (4 mg; GHG-FGF4 complex, n = 2; GHG-lacZ complex, n = 2) and the original FGF4-gene solution (naked FGF4-gene, n = 2) were diluted with 0.4 ml saline and slowly injected through a 23-gauge needle at a single point in the adductor muscle marked with a 4-0 nylon suture. Tissue samples from the transfected left adductor muscle (the injection site and the adjacent region 10 mm apart from the injection site), the right adductor muscle, stomach, liver, spleen, testes, kidneys, heart, lungs, and brain were retrieved and immediately frozen in liquid nitrogen on day 17; FGF4-gene expression was evaluated by reverse transcription-nested polymerase chain reaction (RT-nested PCR). In the remaining 10 rabbits, gene expression was evaluated with lacZ gene; GHG-lacZ complex (n = 5) and naked lacZ solution (n = 5) were injected at a single point in the adductor muscle in the same way as the GHG-FGF4 injection on day 10. On day 17, a muscle sample at the injection site was dissected out, and expression of lacZ was determined by X-Gal histostaining (14).

PROTOCOL 2: SALVAGE OF HINDLIMB ISCHEMIA WITH GHG-PLASMID COMPLEX ENCODING FGF4. The angiogenic effect of three sets of GHG-DNA complexes were compared in 39 rabbits with hindlimb ischemia: 1) GHG impregnated with lacZ plasmid (GHG-lacZ: control); 2) naked FGF4-plasmid (naked FGF4-gene); and 3) GHG impregnated with FGF4 plasmid (GHG-FGF4). The amount of plasmid was 500 μg (1.0 ml) and that of GHG was 4 mg. On day 10 of ischemia, the gene complex was injected at five points 20 mm apart in the adductor muscle with a 23-gauge needle.

In 18 rabbits, on days 10 and 38 of ischemia, calf systolic blood pressure was measured by the Doppler flow signal from the posterior tibial artery (ES-100V2, Hayashi Denki Co., Kawasaki, Japan) with a 25-mm wide cuff. The calf blood pressure ratio of each rabbit was defined as the ratio of the systolic pressure of the ischemic limb to that of the normal limb. Regional blood flow was measured by the microsphere method (15) at baseline on days 0 and 38. On day 38, adenosine (100 μg/kg/min) was administered 30 min after baseline flow measurement (vasodilatory condition). A 4F catheter was introduced into the ascending aorta via the common carotid artery for microsphere injection and adenosine administration. Microspheres (15-μm diameter, 3 × 106) labeled with one of four sets of stable heavy elements (In, I, Ba, or Ce, Sekisui Plastic, Osaka, Japan) (15) were suspended in 0.05% sodium dodecyl sulfate at a concentration of 5 × 106/ml and injected into the ascending aorta. After killing the animals, the adductor, semimembranous, and gastrocnemius muscles were dissected out and weighed. The X-ray fluorescence of the labeled microspheres was measured in 4 to 8 g of the dissected muscles to calculate the regional blood flow (15) and expressed as the ratio of flow in the ischemic limb to flow in the normal limb.

JACC Vol. 41, No. 6, 2003
March 19, 2003:1056–62

**Table 1.** Morphologic Evaluation of Gene Therapy

| Muscle Necrosis (Area) | GHG-lacZ | Naked FGF4 | GHG-FGF4*† |
|---|---|---|---|
| Grade 0 (0 $cm^2$) | 0 | 0 | 0 |
| Grade 1 (<1 $cm^2$) | 0 | 0 | 50% (3/6) |
| Grade 2 (<3 $cm^2$) | 17% (1/6) | 33% (2/6) | 50% (3/6) |
| Grade 3 (<5 $cm^2$) | 0 | 67% (4/6) | 0 |
| Grade 4 (<10 $cm^2$) | 50% (3/6) | 0 | 0 |
| Grade 5 (>10 $cm^2$) | 33% (2/6) | 0 | 0 |
| Muscle weight ratio (%) | 48 ± 67 (6) | 62 ± 14 (6) | 79 ± 11* (6) |

Morphologic indexes in 18 gene-transferred rabbits on day 38. The ischemic limb was macroscopically evaluated by using graded morphological scales for muscle necrosis area (the adductor, semimembranous, medial large, and gastrocnemius muscles) (grade 0 to 5); GHG-FGF4 group had significantly less muscle necrosis compared with naked FGF4 and GHG-lacZ groups. Muscle weight ratio was significantly different between GHG-FGF4 and GHG-lacZ groups. $p < 0.05$ vs. *GHG-lacZ, †naked FGF4 (Kruskal-Wallis test, analysis of variance).

FGF4 = fibroblast growth factor 4; GHG = gelatin hydrogel; lacZ = β-galactosidase.

Sufficient mixing of microspheres injected into the aorta (not into the left atrium) was confirmed by a preliminary study in which two different sets of microspheres were simultaneously injected into the aorta. The liner regression analysis on the two different sets of flows yielded an almost identical regression line ($y = 1.011x - 0.003$, $r = 0.98$, $Sy \cdot x = 0.032$ ). The remaining muscle tissue was used for histological analysis. An investigator blinded to the treatment macroscopically evaluated the ischemic limb on graded morphological scales for area of muscle necrosis (the adductor, semimembranous, medial large, and gastrocnemius muscles; grade 0 to 5; Table 1).

Synchrotron radiation microangiography characterized by high-resolution and high-sensitivity (16) was performed in 21 rabbits as previously described (15,17,18). The system is capable of separating adjacent lead lines only 20 μm apart on the resolution bar chart with 640× higher sensitivity than charge-coupled device camera system. This system allows detection and functional analysis of small vessels with a diameter of 200 to 500 μm in situ (15,17,18). Contrast material containing 37% nonionic iodine (Iopamidol, Nihon Schering Co., Tokyo, Japan) was injected via a 4F catheter placed immediately above the aortic bifurcation under baseline condition and during adenosine administration (100 μg/kg/min) (vasodilatory condition) via the same catheter. Vessel density in the midzone collateral was evaluated as an angiographic score (11,15,18).

**Plasmid.** Complementary deoxyribonucleic acid (cDNA) of human hst1/FGF4 (19), or bacterial β-galactosidase was inserted into the expression vector pRC/CMV (Invitrogen Corp., Carlsbad, California) and designated as pRC/CMV-HST1-10 (human stomach tumor) and pRC/CMV-lacZ, respectively. Preparation and purification of the plasmid from cultures of pRC/CMV-HST1-10-, or pRC/CMV-lacZ-transformed *Escherichia coli* were performed by centrifugation to equilibrium in cesium chloride-ethidium bromide gradients.

**RT-nested PCR.** Ribonucleic acid (RNA) was extracted from tissues with ISOGEN (Nippon Gene, Tokyo, Japan). The extracted RNA was treated with DNase twice to eliminate DNA contamination. In each set of experiments, 0.5 μg of total RNA was denatured at 70°C for 5 min, and reverse transcription was carried out at 37°C for 60 min; RT-nested PCR was carried out in a thermal cycler (GeneAmp PCR System 9600, Perkin Elmer, Wellesley, Massachusetts) with primers designed to selectively amplify the FGF4 cDNA. The external primers EcoHST1f3 (forward primer: GGA ATT CAC TGA CCG CCT GAC CGA CGC ACG GCC CTC G) and SalHST1r2 (reverse primer: GCG TCG ACC CCG AGG CTG AGG CAA GGG TCC TCT) were used for the first round (generating a 704-base pair [bp] fragment). The second round of the amplification (nested PCR) was performed with two internal primers HST1LGC1 (forward primer: AGC TCT CGC CCG TGG AGC GG) and HST1AA-r (reverse primer: CTC TGG AGG GTC ACA GCC TG) (generating a 282-bp fragment). The PCR reactions were performed as follows. The thermal cycle conditions for the first round were 30 cycles (95°C for 1 min, 59°C for 1 min, 72°C for 1 min), and for the second round were 25 cycles (94°C for 1 min, 72°C for 2 min), followed by incubation at 72°C for 10 min, respectively. Amplification products were detected after electrophoresis on 3.5% agarose gels by staining with ethidium bromide. A primer set of beta-actin (generating a 506-bp fragment) was used as a positive control for RT-PCR analysis.

**Statistical analysis.** Data are presented as mean values ± SD. Differences were assessed by using the paired *t* test, Kruskal-Wallis test, or analysis of variance (ANOVA) for factorial or repeated measures with the Scheffé F test when applicable. A value of $p < 0.05$ was considered statistically significant.

## RESULTS

**Protocol 1: DNA degradation and the improvement of transfection efficiency by GHG.** The radioactivity of radiolabeled DNA impregnated into GHG in the limb muscle remained above the detection limit for four weeks (solid line in Fig. 1). The radiolabeled DNA impregnated into GHG had decay sequences almost identical to those of the radiolabeled GHG (dotted line in Fig. 1). By contrast, the radioactivity of naked DNA (dashed line in Fig. 1) decreased to <10% of the baseline within a day.

Gelatin hydrogel improved transfection efficiency in vivo; RT nested-PCR analyses revealed FGF4 expression at all injection sites in the left adductor muscle in the FGF4-gene-treated animals (n = 4), as shown in lanes 1 (naked FGF4-gene) and 4 (GHG-FGF4) in Figure 2; FGF4 expression was also detected in the adjacent region 10 mm apart from the injection site in the left adductor muscle in the GHG-FGF4-treated animals (lane 5), but not in the naked FGF4-gene-treated animals (lane 2). No expression was detected in any animal at remote sites, such as the right adductor muscle (lanes 3 and 6), stomach, liver, spleen,

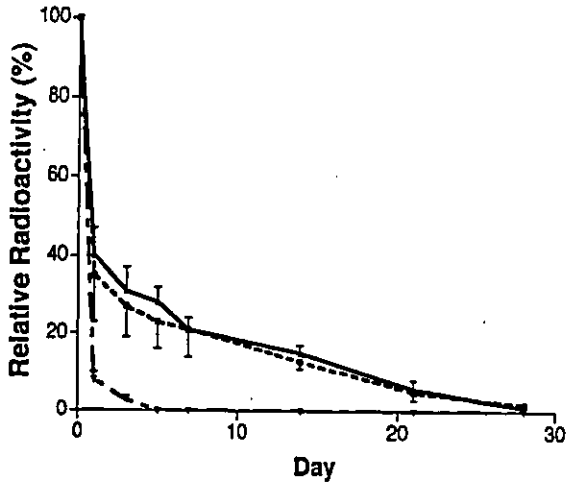


**Figure 1.** Decay sequences of radiolabeled deoxyribonucleic acid (DNA), gelatin hydrogel (GHG), and DNA combined with GHG in the hindlimb muscles of mice. Unlabeled GHG impregnated with $^{125}$I-labeled DNA (**solid line**), $^{125}$I-labeled GHG (**dashed line**), and $^{125}$I-labeled DNA solution (**dotted line**) were injected into the hindlimb muscles.

testes, kidneys, heart, lungs, or brain (data not shown); lacZ-treated animals showed no FGF4 expression at any sites (lanes 7 and 8). Beta-actin expression was detected in all samples (lower panel), but neither beta-actin nor FGF4 expression was detected in any control samples that were not treated with reverse transcriptase; lacZ expression of naked DNA (500 $\mu$g) was localized to the injection site (Fig. 3A), whereas GHG-DNA complex (DNA amount 500 $\mu$g) showed a spatially expanded expression on day 17 (Fig. 3B). The degree of gene expression in myocytes was also augmented by GHG.

**Protocol 2: salvage of hindlimb ischemia with GHG-plasmid complex encoding FGF4.** Functional evaluation of ischemic hindlimbs showed amelioration of the ischemia

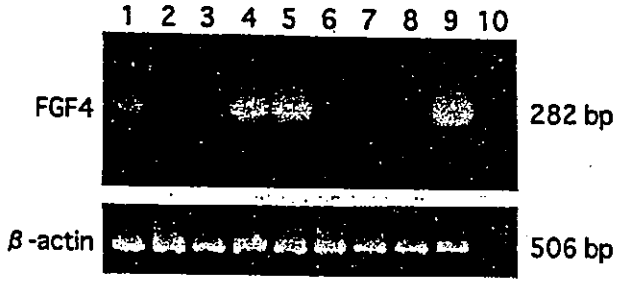


**Figure 2.** Representative transgene expression demonstrated by reverse-transcription nested polymerase chain reaction (RT-nested PCR). The left adductor muscle of the rabbits was injected with naked fibroblast growth factor 4 (FGF4) gene (**lanes 1 to 3**), gelatin hydrogel (GHG)-FGF4 (lanes 4 to 6), or GHG-lacZ (**lanes 7 and 8**). Each sample was obtained from the injection site (**lanes 1, 4, and 7**) and the adjacent region 10 mm apart from the injection site (**lanes 2, 5 and 8**) in the left adductor muscle, and from the contralateral adductor muscle (**lanes 3 and 6**). The RT-nested PCR products from ribonucleic acid of each sample were analyzed on agarose gel; FGF4 expressed Cc1/l6 cells as a positive control (lane 9) and no deoxyribonucleic acid (DNA) template as a negative control (lane 10). A housekeeping beta-actin gene was amplified as a complementary DNA loading control.

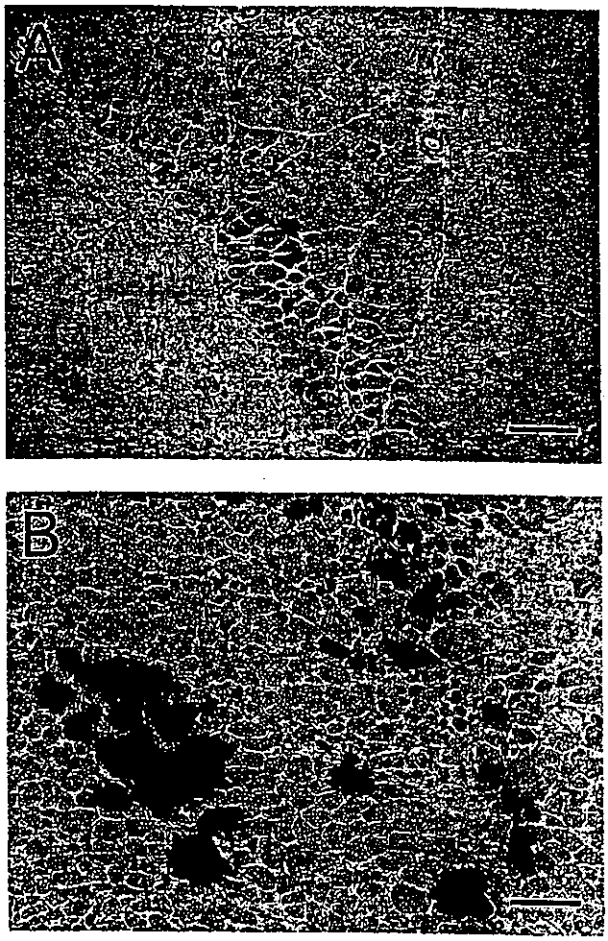


**Figure 3.** Representative gene expression of lacZ in the ischemic adductor muscle in rabbits on day 17. Naked deoxyribonucleic acid (DNA) (**A**) or gelatin hydrogel-DNA complex (**B**) was injected into the adductor muscle 10 days after the ischemic insult. X-Gal stain; original magnification ×20; bar = 200 $\mu$m.

by the FGF4-gene and potentiation of the amelioration when GHG was used as a delivery device. The augmentation of regional blood flow with GHG was more evident under vasodilatory conditions than at the baseline.

Regional blood flow analysis and angiographic analysis further confirmed the background mechanism for amelioration of hindlimb ischemia by GHG-FGF4 (Table 2). On day 38, blood flow during adenosine administration (vasodilatory condition) in the GHG-FGF4 group (105 ± 13% in terms of ischemic/normal flow ratio) was significantly higher than in either the naked FGF4-gene group (68 ± 18%, $p < 0.05$) or the GHG-lacZ group (50 ± 12%, $p < 0.05$, ANOVA). The differences between the naked FGF4-gene and GHG-lacZ groups were not significant (ANOVA). The adenosine-dependent flow-augmentation (responsiveness to vasodilatory stimulation; comparison between adenosine and baseline values on day 38) was noted only in the GHG-FGF4 group (from 79 ± 16% to 105 ± 13%, $p < 0.05$, ANOVA), and not in the other two groups. A similar tendency was noted in flow under baseline conditions on day 38 in all three groups; however, the